HOW DOES THE SOLAR WIND POWER THE MAGNETOSPHERE DURING GEO-EFFECTIVE HIGH SPEED STREAMS?

Mona Kessel and Xi Shao
NASA Goddard Space Flight Center

Abstract. We show two types of solar energy flux that with high probability, couple to the Earth's magnetosphere and cause enhanced magnetospheric fluctuations. 70-80 R_E upstream from Earth, Wind observations show significant, sustained power at Pc5 frequencies intrinsic to a high speed stream starting March 29, 2002. The enhanced power is evident in dynamic pressure fluctuations and to a lesser extent in compressional magnetic field fluctuations. This high speed stream is not associated with a large magnetic storm, but strong Pc5 pulsations are observed at geostationary orbit. Geotail observations near the magnetopause show enhanced compressional power at Pc5 frequencies, especially at the nose and on the dawn flank, both in the magnetosheath and the adjacent boundary layer. The observations suggest that more energy may be transferred across the nose than at the flanks during high speed streams. The sustained dynamic pressure fluctuations may be responsible for the sustained geomagnetic pulsations seen at GOES 8 in the noon and midnight sectors, although the midnight sector might have additional sources. GOES 8 observations of dawn pulsations follow the trend of the compressional magnetic field fluctuations, that is higher at first and then reduced. Compressional magnetic field fluctuations may control the level of Pc5 pulsations on the dawn side. Northward IMF along with Geotail observations of magnetopause motion and MHD simulations of vortices along the flanks suggest that a Kelvin-Helmholtz (K-H) instability may contribute to transport of the compressional energy into the magnetosphere.

1. Introduction

The solar wind supplies the energy to drive many magnetospheric processes. Various standard indices have been developed that are measures of specific geomagnetic activity, e.g., storm indices such as D_{st} and substorm indices such as AU, AL, AE. Solar-wind-magnetospheric coupling studies have related solar wind input to geomagnetic activity through empirical formulae. Akasofu [1981], building on analysis by Perreault and Akasofu [1978] developed a first approximation for a solar wind-magnetosphere energy coupling function. They theorized that there were two forms of solar energy flux, ρV^3 and VB^2. Both are pressure related, the former dynamic pressure and the latter compressional MHD waves or fluctuations. Akasofu and Chapman [1963] found no obvious correlation between ρV^3 and geomagnetic activity so Akasofu's first approximation depended on solar wind compres-

sional wave flux and IMF direction. This function correlated with the energy consumption rate of the magnetosphere that they defined as depending on D_{st} and AE indices.

Earth's magnetosphere's is made up of magnetic fields from different sources and involves a complicated set of processes: storms, substorms, current flows, and power redistribution. It is generally accepted that storms are driven by the solar wind. Much attention has focused on Coronal Mass Ejections (CME's) especially during the recent solar maximum when CME's were prevalent and caused large solar storms. Tsurutani and Gonzalez [1994] discussed the causes of geomagnetic storms during solar maximum, primarily focusing on CME's. Li et al. [2003] claimed that the declining phase of the solar cycle is the most geo-effective phase. They equated geo-effectiveness to strong increases in two parameters: outer radiation belt flux or so-called "killer" electrons (SAMPEX 2-6 MeV electrons) and the D_{st} index of the strength of magnetic storms. Their Figure 1 illustrates the strength of their claim for the last solar cycle with the strongest negative D_{st} and electron fluxes occurring during the declining phase. The declining phase of the solar cycle is characterized by long-lasting recurrent high speed solar wind streams, many leading to strong magnetic storms. Li et al. [2003] suggest that CME's don't occur as often or last as long as high speed streams and thus are not as geo-effective.

Many papers have shown a linkage between high speed solar wind streams, "killer" electrons and ULF waves [e.g., Rostoker et al., 1998, Baker et al., 1998, Mathie and Mann, 2000]. Kessel et al. [2003] showed that the high speed streams carry enhanced Pc5 power as compressional fluctuations (1-8 mHz). They also showed a clear correlation between the enhanced Pc5 power in the solar wind streams and enhanced Pc5 power in the magnetosphere as determined from the Kilpisjarvi ground station. Their figures 2 and 3 showed the correlation for power in the magnetic field parallel and transverse components, respectively. These fluctuations are not generated in the foreshock because they are initially observed at Wind, 200 R_E upstream from Earth. The Pc5 power may be more geoeffective than that in the Pc3/4 range. Lower frequency peaks (from a few 10^{-7} Hz to mHz) also exist in high speed streams as is typical of the solar wind spectrum for both magnetic field fluctuations [e.g., Goldstein et al. (this issue)] and speed fluctuations [e.g., Burlaga and Forman, 2002].

It is commonly agreed that toroidal Pc5 pulsations are caused by an external source in the solar wind. The most frequently cited source of Pc5 pulsations in the magnetosphere is the Kelvin-Helmholtz instability at the magnetopause [e.g., Dungey, 1955; Miura, 1992; Anderson, 1994; Engebretson et al., 1998]. Mann et al. [1999] have recently shown that for very large flow speeds at the magnetopause flanks, the Kelvin-Helmholtz instability can energize body type waveguide modes. Other possible sources of Pc5 pulsations have been proposed such as upstream shock-related pressure oscillations that drive magnetopause surface waves with periods in the Pc5 range [Sibeck et al., 1989]. Fairfield et al. [1990] suggested that upstream pressure variations may be linked to magnetospheric compressions. Engebretson et al. [1998 and sources therein] suggested that if the compression regions at the leading edges of high speed streams contain waves in the Pc5 range they could provide a source of wave energy to the magnetosphere or that the waves could act as seed perturbations to drive boundary displacements that are amplified by the Kelvin-Helmholtz instability. By contrast, Kepko et al. [2002] showed observations of pressure fluctuations at the same discrete frequencies in the solar wind as in the magnetosphere and suggested that the solar wind may be a direct source for discrete Pc5 pulsations. Wright and Rickard

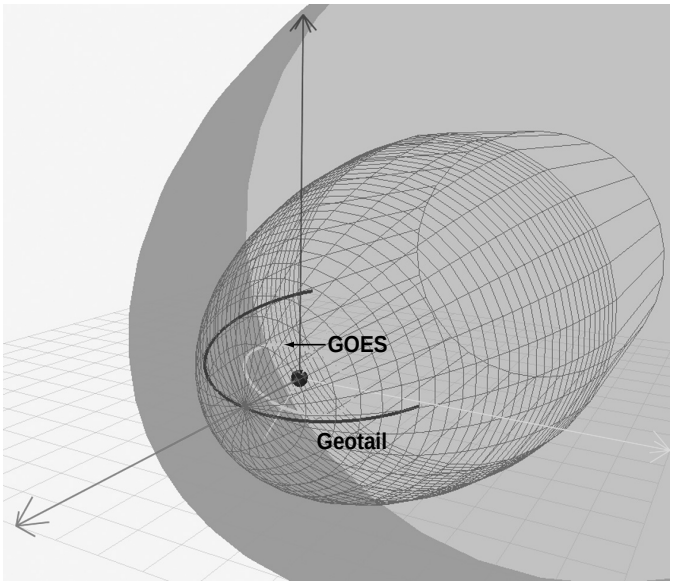

Figure 1: View from Wind satellite with Geotail skimming the magnetopause and GOES at geostationary orbit.

[1995] showed that broadband fluctuation power in the solar wind can lead to enhanced excitation of the magnetospheric cavity or waveguide modes, even if the spectral content of the upstream and magnetospheric waves are different.

In the next section we briefly describe our data and methodology. We then show observations of fluctuations in the solar wind and near the magnetopause, and pulsations at geostationary orbit for one high speed stream in 2002. We suggest here that the solar wind input for this high speed stream is first dependent on the Pc5 power in dynamic pressure fluctuations, ρV^2, and to a lesser degree on the Pc5 power in compressional magnetic field fluctuations, B^2. These inputs are sustained for the entire high speed stream as are Pc5 pulsations observed in the magnetosphere at geostationary orbit for the duration of the high speed stream passage. We discuss the local time effects at the magnetopause and inner magnetosphere which highlight the magnetospheric impacts and energy transfer mechanisms.

2. Orbits, Instruments and Methods

For this study we used data from the Wind, Geotail, and GOES satellites for a high speed stream starting 29 March 2002. Wind was upstream between 70 and 80 R_E. Geotail was skimming the magnetopause, crossing between the magnetosphere, boundary layer, and magnetosheath as shown in Figure 1, and GOES was at geostationary orbit. We used data from the Magnetic Field Investigation (MFI) [Lepping et al., 1995] and the Solar Wind Experiment (SWE) [Ogilvie et al., 1995] on Wind. We used magnetometer data from the Magnetic Field Measurement (MGF) [Kokubun et al., 1994] and the Low Energy Particle (LEP) [Mukai et al., 1992] instrument on Geotail. We used the magnetic field instrument on both GOES 8 and GOES 10 [Singer et al., 1996].

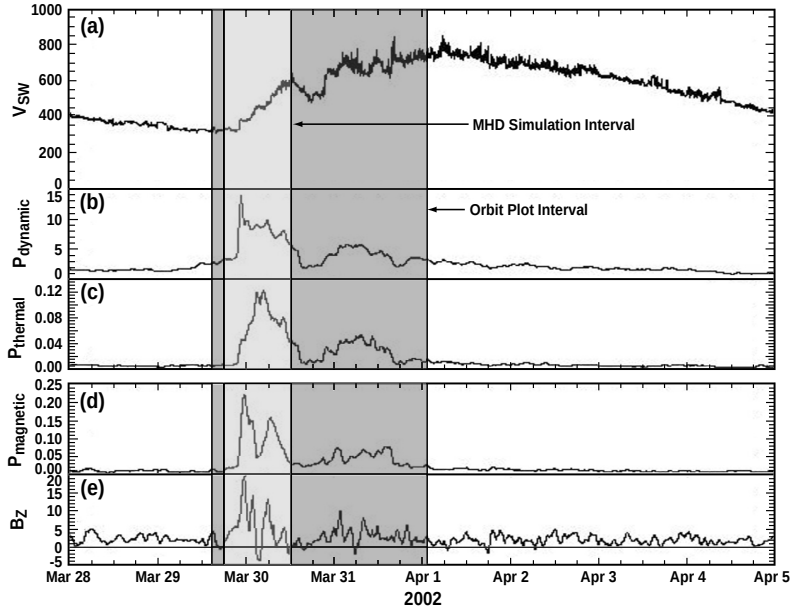

Figure 2: High speed solar wind stream (Wind data). Two nested intervals are shown (arrows indicate end points). The longer interval corresponds to the orbit shown in Figure 1 and the shorter (lighter in color) interval corresponds to the MHD simulation.

For the solar wind spectral analysis we used both dynamic pressure (nV_{sw}^2) and magnetic field magnitude (compressional waves). The pressure was converted to the same units as the magnetic field (nT) in order to compare quantitatively as well as qualitatively. Near the magnetopause (Geotail) and in the magnetosphere (GOES) we used magnetic field magnitude (compressional fluctuations) to compare with the solar wind fluctuations. We used 1 minute resolution data to provide detail on the Pc5 portion of the spectrum (1-8.3 mHz). Each data set was detrended by subtracting the background field using the IDL smooth function with a window of 61 points (one hour). Other windows from 20 minutes to 4 hours were examined for comparison; the spectral analyses were not significantly different. The resulting fluctuations were tapered using a Parzen window. The data were processed using a fast Fourier transform algorithm with a sliding 128 point (2 hour) window to create power spectral densities (PSD) and then the PSDs were summed from 1 to 8.3 mHz to get total power in the Pc5 range. FFT methods were determined from Ramirez [1985] and Press et al. [1986].

We used the Lyon-Fedder-Mobarry (LFM) global MHD code [Fedder et al., 1995] to examine plasma flows and vortices. The code couples a 3D MHD magnetospheric model with a 2D electrostatic ionospheric model and was then driven by solar wind input provided by satellite data.

3. Observations

The top panel of Figure 2 begins with a nominal solar wind followed by a high speed stream at the end of March 29, 2002. The high speed stream is identified by an initial

increase in speed with the speed remaining high for 2 days before gradually trailing off over 3 days. At the leading edge of the stream there is a compression region as seen by the increases in dynamic pressure, thermal pressure and magnetic pressure in panels (b) - (d). This compression region occurs at the onset of the increase in speed and is evident 3/4 of a day. There is a second increase in pressure of smaller magnitude also evident for about 3/4 of a day. Then the pressures return to a nominal value where they remain for the remainder of the high speed stream. We indicate the interval corresponding to the orbit of Geotail shown in Figure 1. This interval encompasses the two compression regions just discussed. We also indicate the interval corresponding to an MHD simulation run using the LFM model that corresponds to the first compression region. We will discuss both data from the MHD simulation and from satellite observations later in this section.

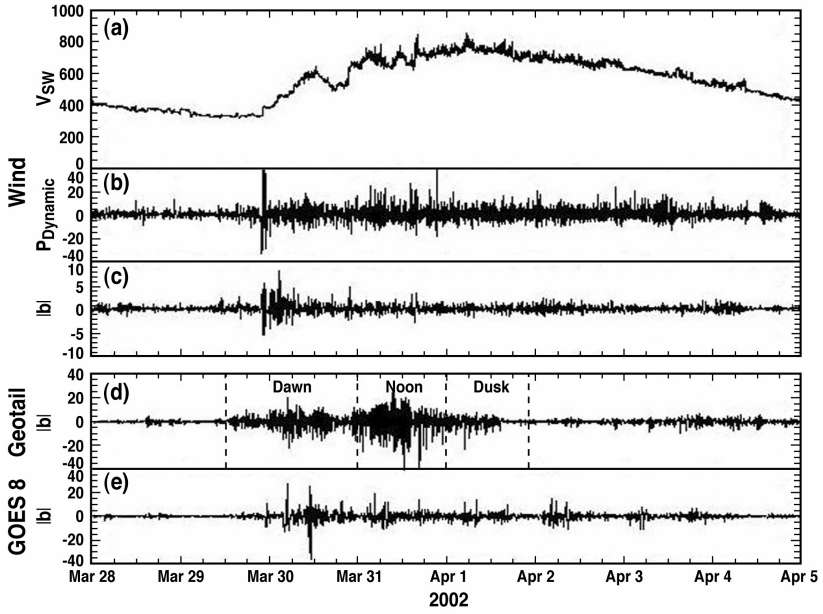

Figure 3: Compressional ULF fluctuations during high speed solar wind stream 28 March - 5 April 2002.

We next look at the fluctuations associated with this high speed stream in Figure 3. The top panel shows the speed again to orient the viewer. For the dynamic pressure (b) and magnetic field magnitudes (c - e), we detrend the data by stripping out the background. The resulting fluctuations intrinsic to the solar wind are shown in panels (b) and (c) of Figure 3, and those in the magnetosphere in (d) and (e). The pressure fluctuations have been converted to the same units (nT) as the magnetic field fluctuations so that they can be compared quantitatively as well as qualitatively. In the solar wind, the fluctuations in the dynamic pressure are larger than those in the magnetic field and are sustained at a higher level throughout the entire high speed stream interval. The fluctuations in the magnetic field magnitude are largest in the compression region at the onset of the high speed stream and are maintained at a lower level for the remainder of the high speed stream.

We compare the solar wind fluctuations with those near the magnetopause and in the

magnetosphere in the bottom two panels of Figure 3. Panel (d) shows fluctuations in the magnetic field magnitude at Geotail which is skimming the magnetopause during the first part of this interval as seen in Figure 1. The fluctuations are highest near the nose of the magnetopause. The fluctuations on the dawn flank are less than those at the nose but more than those at dusk. These regions are indicated in Figure 3(d). Geotail is crossing between the magnetosheath and boundary layer during this interval as will be discussed later. Figure 3(e) shows fluctuations at GOES 8 inside the magnetosphere at geostationary orbit. These fluctuations are higher during the passage of the high speed stream compared to during times of nominal solar wind (March 28-29), and highest during the first compression region ending March 30 ~1500.

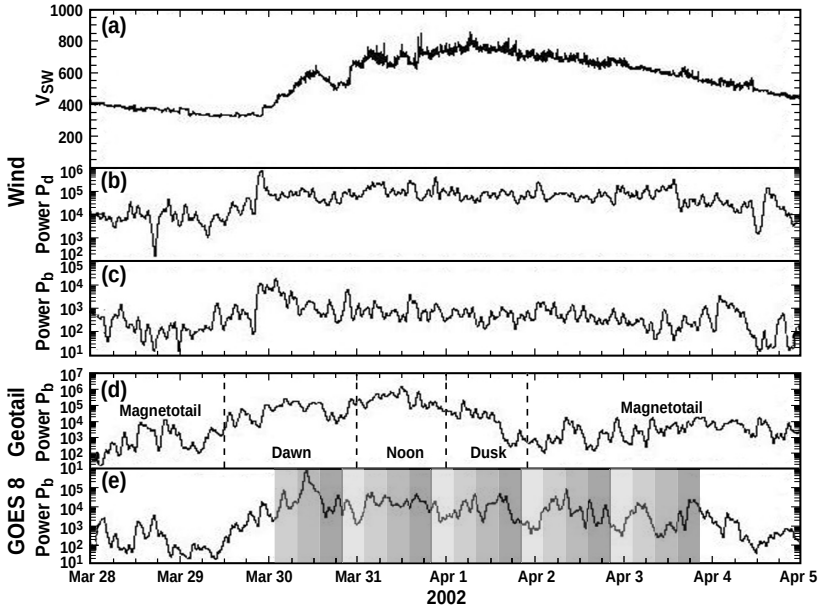

Figure 4: Top panel shows high speed solar wind stream on 28 March - 5 April 2002. (b) shows Pc5 power in solar wind dynamic pressure fluctuations. The lower 3 panels show Pc5 power in compressional magnetic field fluctuations (c) in solar wind, (d) near magnetopause (Geotail), and (e) at geostationary orbit in 6 hour strips at midnight, dawn, noon, and dusk.

Figure 4 shows the power in these various fluctuations along with the solar wind speed in the top panel to orient the viewer. The power was determined by performing a FFT on the fluctuations shown in Figure 3. The power in all cases was enhanced in the Pc5 frequency range (1-8.3 mHz) during high speed streams. Power was also evident at lower frequencies as in a typical IMF spectrum, but we focus on the Pc5 frequency range as it appears to be more geo-effective. We first examine the power intrinsic to the high speed stream in panels (b) and (c). The power in the dynamic pressure (b) is larger by at least an order of magnitude compared to the power in the magnetic field compressional component (c). The power in the dynamic pressure is also sustained for the entire interval of the high speed stream compared to the power in the magnetic field compressional component which is highest at the beginning of the stream, and then reduced. Near the magnetopause and inside the magnetosphere the power is enhanced during the passage of the high speed stream

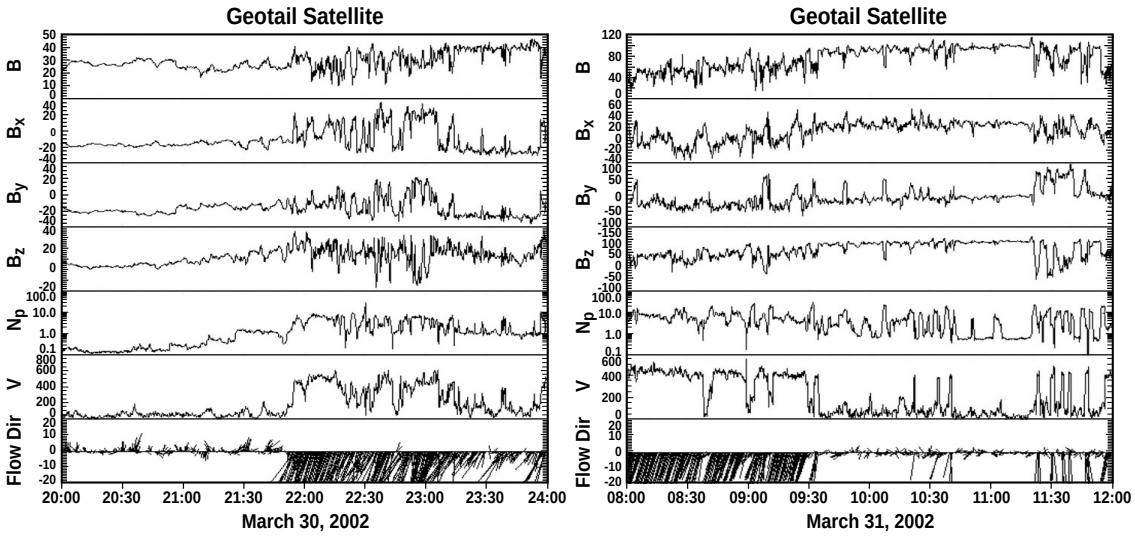

Figure 5: Magnetic field and plasma characteristics near the magnetopause (a) on the dawn flank (4-5 LT) and (b) at the nose (10-12 LT).

as shown in panels (d) and (e), respectively, of Figure 4.

As discussed in reference to Figure 3 the power at Geotail shown in Figure 4(d) is enhanced most significantly near the nose of the magnetopause (noon), followed by the dawn and dusk flanks, respectively. The power in the magnetotail region may be slightly enhanced during the high speed stream compared to in the solar wind, though no analysis of this region was undertaken in this study. Figure 4d shows some peaks and valleys in the power as Geotail was skimming the magnetopause on March 30 and 31, and April 1. Geotail was crossing back and forth between the magnetosheath and the boundary layer; generally the power in the magnetosheath was higher than in the adjacent boundary layer. The depressions within each region occur in the boundary layer. We show Geotail boundary crossings below.

At GOE8 (Figure 4e), the power during the passage of the high speed stream is enhanced compared to the interval of nominal solar wind. We further subset the data in Figure 4e into adjacent 6 hour strips to look for local time effects. The midnight sector is identified as a series of light gray strips, the dawn sector is shown as slightly darker strips, the noon sector is darkest strips, and the dusk sector is white. The geostationary power just preceding the onset of the high speed stream shows equal peaks pre-midnight, at dawn and at the nose, with significantly less power elsewhere. During the passage of the high speed stream, the largest enhancement is in the first dawn strip on March 30. Subsequent dawn strips show no enhancement compared to adjacent regions and even a decrease mid-stream and on. The midnight region is at about the same level throughout the passage, but slightly weakening as time goes on. The noon region (darkest strips), like the midnight region, is enhanced throughout though it often has a double peak and power is slightly less than at midnight. Full characterization of these pulsations is outside the scope of this paper, but we discuss possible source regions in the next section.

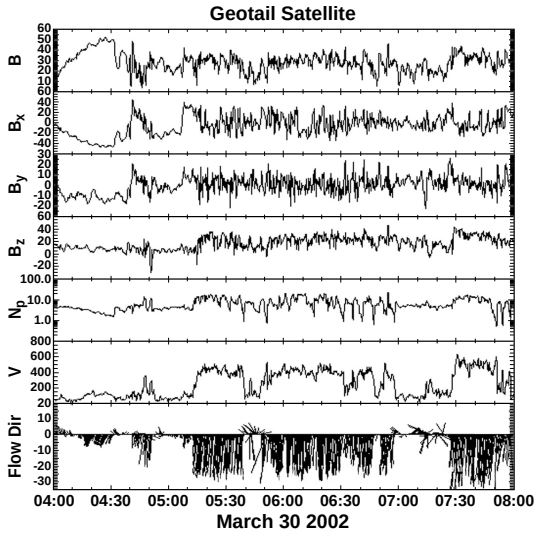

Figure 6: Geotail data on the dawn side flank of the magnetopause.

We next examine, in more detail, Geotail data in the vicinity of the magnetopause on the dawn flank and at the nose. During March 30 and 31 Geotail was crossing back and forth between the magnetosheath and the boundary layer. Figure 5 shows two time intervals during these two days: (a) shows data from the dawn flank between 04 and 05 LT (x from -5 to -10R_E on the nightside) and (b) shows data near noon (10 to 12 LT). Both (a) and (b) show the magnetic field magnitude and cartesian GSE coordinates (top four panels) followed by the ion density, speed and flow direction from the LEP instrument. The flow direction (bottom panels) is in the $+(-)x$ direction if pointing up (down) and in the $+(-)y$ direction if pointing right (left). The magnetosheath is identified by turbulent magnetic fields, high density and speed, and flows (on the flanks) primarily in the $-x$ direction. The boundary layer is distinguished by more orderly magnetospheric fields, low densities and speeds, and random flow directions. Figure 5a shows the last four hours of March 30. Geotail was in the boundary layer at 2000 and crossed into the magnetosheath around 2200 followed by multiple traversals between the two regions. Figure 5b shows four hours of March 31. Geotail was in the magnetosheath at 0800 with a couple of short forays into the boundary layer before moving into the boundary layer at about 0930. Multiple traversals back into the magnetosheath are evident later in this interval. The magnetic field fluctuations in the boundary layer between 2000 and 2200 were less than in the magnetosheath and later boundary layer regions in both (a) and (b). It may be that there are more fluctuations and power in the boundary layer near the nose than on the flank. We discuss this in the following section.

We also show an interval of Geotail data from earlier on March 30, 2002 in Figure 6 when Geotail is at about (-20, -15)R_E on the dawn flank. The magnetic field and plasma parameters from 0400 to 0800 are in the same format as Figure 5 and likewise show multiple traversals between the magnetosheath and boundary layer. The solar wind pressure is very high at this time (Figure 2) so that the magnetopause is contracted. The magnetopause contraction also explains why Geotail remained near the dawn flank much longer than it was

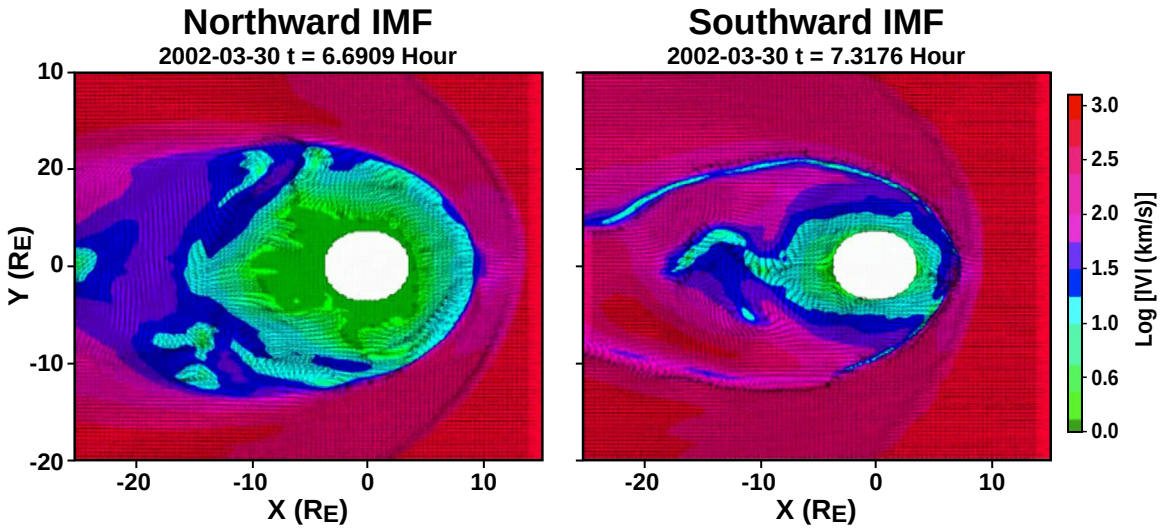

Figure 7: Typical MHD flows under (left) northward and (right) southward IMF.

on the dusk flank when the magnetosphere had relaxed back to its more nominal position. The IMF was strongly northward and the solar wind speed was increasing from about 400 to 600 km/s during this interval. The speed as observed by Geotail varied between less than 50 km/s and 600 km/s. The density was highly variable especially from 0510 to 0700, including during intervals that would be labeled as magnetosheath by other features (high speed with fairly constant flow direction and turbulent fields). The regions of highly variable density may not be easily classified as either magnetosheath or boundary layer, but may represent mixing regions. It is common to find turbulent regions behind the quasi-parallel bow shock and makes study of this region problematic. It is clear that the boundary is in motion; the boundary may also be wave-like as Geotail is skimming through.

Figure 2 showed an interval for which an MHD simulation was run. During this interval the solar wind speed started at a nominal value around 300 km/s and increased to about 600 km/s. The IMF was northward for much of this period and the dynamic, thermal and magnetic pressure all increased dramatically. We focused on plasma flows produced from the MHD simulation, and found a distinct difference between flows during times of northward and southward IMF. Figure 7 shows typical MHD flows under (left) northward and (right) southward IMF. The background is the colormap of the log of the velocity magnitude (speed). Black arrows indicate the flow direction of unit length in the equatorial plane. Under northward IMF large scale vortices developed and were swept downtail with the solar wind flow, and stagnant regions formed (Figure 7 left). At the top and bottom of this MHD snapshot, vortical regions can be seen as darker green regions of small V surrounded by regions of light blue and then darker blue (increasing V). Black arrows in these regions indicate circular flow; these can be seen more clearly in Figure 8 which is a 3D depiction of one vortex region.

Under southward IMF a thin boundary layer region was evident (Figure 7 right) and the magnetospheric region was compressed compared to times of Northward IMF. In this MHD

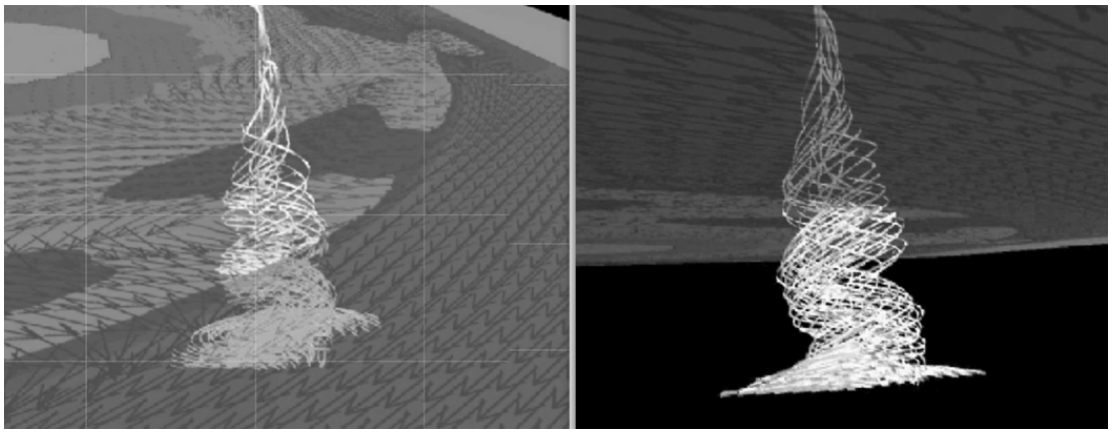

Figure 8: 3-dimensional vortex produced during northward IMF pictured from (a) above and (b) below the ecliptic plane.

snapshot, the thin boundary layer at the top (dusk) can be seen clearly, but the boundary layer at the bottom (dawn) appears broken. At other times of southward IMF, the MHD snapshots show a clear dawn side boundary layer. Referring back to the B_z component of IMF shown in Figure 2, the simulation results looked like those in Figure 7 (left) for about the first third of the run (northward IMF). This was followed by a few hours of southward IMF where the results looked like Figure 7 (right). The remainder of the MHD run consisted of a few more hours of northward IMF and a few short southward intervals. The vortices shown in Figure 7a could be associated with a Kelvin-Helmholtz type instability. The Geotail data on the dawn side around this time is highly turbulent and does not allow easy identification of K-H features, but also does not preclude K-H. Most observations of K-H instabilities have been made on the less turbulent dusk flank [e.g., Fairfield et al., 2000; Fairfield et al., 2003; Hasegawa et al., 2004]. The turbulence and plasma mixing are kinetic effects, not fluid effects and so do not show up in MHD simulation.

Finally, we introduce a new analysis that may be useful in understanding energy transfer across the magnetopause. We show one vortex from our MHD simulation as a 3D object in Figure 8 from (a) above and (b) below the ecliptic plane. Vortices examined from the interval of this MHD simulation are located just inside the magnetopause surface and extend above and below the ecliptic plane a few Earth radii. The one shown in Figure 8 flows in a counterclockwise direction but others flow clockwise. This vortex appears to form below the ecliptic plane and then dissipate into a small region above the ecliptic plane. At this time there were four vortices evident on the dawn flank. Vortices also formed on the dusk flank though generally in smaller number. We are left with many questions from this initial sample. For example, do counterclockwise vortices always form below the ecliptic plane and clockwise vortices above the plane? Is the axis of the vortex always in the z-direction? This tantalizing view of a 3D vortex structure opens up new avenues to pursue. We hope that further exploration in this area will result in a better understanding of the structure of the magnetopause and the energy transfer into the magnetosphere.

4. Summary and Conclusions

Previous studies have shown that Earth's magnetosphere is particularly geo-effective during the declining phase of the solar cycle due to recurrent high speed solar wind streams [e.g., Li et al, 2003]. Many high speed streams are associated with large magnetic storms and D_{st} of -120 to -200 [e.g., Posch et al., 2003], triggered by a southward turning of the IMF usually preceded by a long interval of northward IMF. Some high speed streams do not have large southward IMF or large D_{st} and yet have significant Pc5 pulsations and energetic electrons [Kessel et al., 2004]. The high speed stream in this paper was one of the latter cases, D_{st} was modest, only reaching about -40 (see, e.g., OMNIWeb.gsfc.nasa.gov). One solar wind driver that is consistent across all high speed streams is ULF waves or fluctuations. Akasofu [1981] identified two types of solar energy flux, essentially compressional magnetic field and dynamic pressure fluctuations, that carry energy in the ULF band. He was primarily focused on magnetic storms and correlated compressional magnetic field fluctuations and southward IMF with D_{st} and AE. Kessel et al. [2003] showed 5 months of solar wind high speed streams in 1995 that carried enhanced Pc5 power in compressional magnetic field fluctuations; the solar wind power was correlated with Pc5 power at the Kilpisjarvi ground-based station. In the current paper we have also examined the power in solar wind dynamic pressure fluctuations for one high speed stream in 2002. We are interested here to see how solar energy flux in both compressional magnetic field and dynamic pressure fluctuations affects Earth's magnetosphere for high speed streams without large magnetic storms. A later paper, Kessel et al. [2004] will make comparisons between high speed streams with and without large magnetic storms.

In this paper we have shown power at Pc5 frequencies in the solar wind in both compressional magnetic field and dynamic pressure fluctuations. We first discuss the dynamic pressure fluctuations because they appear to be dominant for high speed streams without large magnetic storms. Power in solar wind dynamic pressure fluctuations remained high for the entire high speed stream shown here and was an order of magnitude higher than power in the largest compressional magnetic field fluctuations (Figure 4). Likewise, Pc5 pulsations observed by GOES 8 overall have higher, sustained power for the entire interval of the high speed stream. But when we look at local time effects with GOES 8 at geostationary orbit, we find that some local time regions have fairly constant sustained power and other regions have more variable power. GOES 8 observations of power in the noon and midnight sectors remained at about the same levels throughout the passage of the high speed stream, with the midnight sector being slighty larger than the noon sector until near the end of the stream interval. Dawn and dusk sectors were variable. The dawn sector showed significant power at the beginning of the stream compared to all other sectors, but then quickly weakened and was less than the power at noon and midnight for the rest of the high speed stream interval. The dusk sector was stronger in the first half of the high speed stream interval and weaker in the second half, but weaker than all other local time sectors at all times during the stream.

At the magnetopause with Geotail data, so far we have examined only compressional magnetic field fluctuations. Without simultaneous measurements in the magnetosheath at dawn, noon, and dusk we cannot tell whether or not compressional magnetic field fluctuations follow the same pattern as in the solar wind, i.e., are strongest at the onset of the high speed stream and then weaken. We expect that dynamic pressure fluctuations will also

be strong in the magnetosheath region, and probably sustained throughout the high speed stream. We have observed that the compressional magnetic field fluctuations vary with local time as Geotail skims the magnetopause; they are highest in the noon sector, followed by dawn, dusk, and then weakest in the magnetotail (Figure 4). The magnetosheath is well known as a turbulent region with most fluctuations originating in the solar wind or associated with the quasi-parallel bow shock [e.g., Crooker et al., 1981; Sibeck et al., 2000]. At the nose of the magnetopause, particles and fields pile up so it is not surprising to find the highest power in this region.

We also used Geotail data to identify magnetosheath and boundary layer regions through both magnetic and plasma characteristics (Figure 5). What we found and show in Figure 4 is elevated power in the boundary layer as well as in the magnetosheath. The power in the boundary layer was less than that in the magnetosheath so only some of the energy crossed the magnetopause. In addition, we found that the power at Pc5 frequencies in the noon boundary layer was higher than that in the dawn or dusk boundary layer. How is this energy transferred to the magnetosphere? Several authors have suggested that pressure pulses drive magnetospheric pulsations [e.g., Sibeck et al., 1989; Fairfield et al., 1990; Engebretson et al., 1998]. The dynamic pressure fluctuations observed by Wind and Geotail were not a pressure 'pulse', but were sustained over many days. Likewise, the magnetospheric pulsations in the noon and midnight sectors were sustained over many days. It is possible that these regions are driven by the fluctuations in dynamic pressure or magnetic pressure and that the energy may enter the magnetosphere in the noon region. This compressional power may decay evanescently farther into the magnetosphere, but be sufficient to reach geostationary orbit. Kepko et al. [2002] suggested that the solar wind may be a direct source for discrete Pc5 pulsations. Alternately, the solar wind/magnetosheath fluctuations at Pc5 frequencies may excite field line resonances (FLR) that are observed at geostationary orbits. Pc5 pulsations are common at latitudes between about 60° and 70° (Hughes, 1994 and sources therein) that map to L-shells that include geostationary orbit. The noon sector GOES 8 observations are more probably explained by one of these scenarios. The midnight sector might also be tied to particle injections from the magnetotail [e.g., Posch et al, 2003 and sources therein]. However, particle injections tend to occur during storm periods and our interval includes only a modest storm as mentioned above.

The dawn sector GOES 8 observations might have a different or additional source than dynamic pressure fluctuations that are sustained at approximately the same level throughout the high speed stream. GOES 8 observations (Figure 4e) showed the strongest dawn pulsations on March 30 from 0800 - 1400 UT; subsequent dawn pulsations observed by GOES 8 were significantly weakened. In this paper we showed solar wind compressional magnetic field fluctuations that were strongest at the onset of the high speed stream (March 29 2000 - March 30 0800), and then decreased by about a factor of 10 for the remainder of the stream (Figure 4c). GOES 8 dawn sector observations were strongest immediately following the strongest solar wind compressional magnetic field fluctuations. This could be a coincidence or it could be that solar wind compressional magnetic field fluctuations drive Pc5 pulsations on the dawn side.

The IMF was strongly northward during most of this interval (March 29 2000 - March 30 0200, and March 30 0400 - 0700), coinciding with vortex formation along the flanks as seen in MHD simulations. The vortices disappeared when the IMF turned southward

(Figure 7). The boundary was in motion as was evidenced by multiple crossings of the magnetopause by Geotail. Engebretson et al. [1998 and sources therein] suggested that solar wind or magnetosheath input waves/fluctuations could act as seed perturbations to drive magnetopause boundary displacements that were amplified by the Kelvin-Helmholtz instability. These can drive geomagnetic pulsations, most likely on the dawn side. A Kelvin-Helmholtz instability can be driven by velocity shear alone at the magnetopause flanks [e.g., Miura, 1984; Otto and Fairfield, 2000]. However, for this high speed stream interval the speed increased and then remained high *after* the strongest dawn pulsations, but the dawn pulsations weakened like the compressional magnetic field fluctuations. It is possible that the solar wind compressional fluctuations control the level of magnetospheric pulsations. A K-H instability could have enhanced the initially driven boundary displacements, and then power was transferred to magnetospheric dawn pulsations. This would account for the various observations, but may not be the only explanation.

In this paper we have shown one high speed stream in 2002 during the declining stage of the current solar cycle. Although more cases must be examined before drawing definitive conclusions we suspect that both types of solar energy flux shown here will be found to be common in high speed streams and will serve as effective drivers of magnetospheric Pc5 pulsations, though they may contribute differently to energizing Earth's magnetosphere. Based on this study we make the following statements. Wind observations showed significant, sustained power at Pc5 frequencies intrinsic to a high speed stream starting March 29, 2002. The enhanced power was evident in dynamic pressure fluctuations and to a lesser extent in compressional magnetic field fluctuations. Geotail observations near the magnetopause suggest that more energy may be transferred across the nose than at the flanks during high speed streams. This energy may be responsible for the sustained geomagnetic pulsations seen at GOES 8 in the noon and midnight sectors, although the midnight sector might have additional sources. GOES 8 observations of dawn pulsations follow the trend of the compressional magnetic field fluctuations, that is higher at first and then reduced, and may control the level of Pc5 pulsations on the dawn side. Northward IMF along with Geotail observations of magnetopause motion and MHD simulations of vortices along the flanks suggest that a Kelvin-Helmholtz (K-H) instability may contribute to transport of the compressional energy into the magnetosphere.

Acknowledgements

We thank R. Boller for his development of the 3D vortex anaylsis. We obtained most of the data for this study from CDAWeb.

References

Akasofu, S.-I., Energy coupling between the solar wind and the magnetosphere, Space Sci. Rev., 28, 121, 1981.

Akasofu, S.-I. and S. Chapman, *J. Geophys. Res.*,68, 125, 1963.

Anderson, B.J, An overview of spacecraft observations of 10s to 600s period magnetic pulsations in the Earth's magnetosphere, in *Solar Wind Sources of Magnetospheric Ultra-Low-Frequency Waves,* edited by M.J. Engebretson, K. Takahashi, M. Scholer, AGU, Wash., D.C., 1994.

Baker, D. N., et al., Coronal mass ejections, magnetic clouds and relativistic magnetospheric electron events: ISTP *J. Geophys. Res.*, 103, 17279-17291, 1998.

Burlaga, L.F., and M. Forman, Large-scale speed fluctuations at 1 AU on scales from 1 hour to 1 year: 1999 and 1995, *J. Geophys. Res.*, 107 (A11), 1403, 2002.

Crooker, N.U., T.E. Eastman, L.A. Frank, E.J. Smith, and C.T. Russell, Energetic magnetosheath ions and the interplanetary magnetic field orientation, *J. Geophys. Res.*, 86, 4455, 1981.

Dungey, J.W., Electrodynamics of the outer atmosphere, in *Proceedings of the Ionosphere Conference*, p. 225, The Physical Society of London, 1955.

Engebretson, M.J., K.-H. Glassmeier, and M. Stellmacher, The dependence of high-latitude Pc5 power on solar wind velocity and phase of high-speed solar wind streams, *J. Geophys. Res.*, 103, 26271, 1998.

Fairfield, D.H. et al., Upstream pressure variations associated with the bow shock and their effects on the magnetosphere, *J. Geophys. Res.*, 95, 3773, 1990.

Fairfield, D.H. et al., Geotail observations of the Kelvin-Helmholtz instability at the equatorial magnetotail boundary for parallel northward fields, *J. Geophys. Res.*, 105, 21159, 2000.

Fairfield, D.H. et al., Motion of the dusk flank boundary layer caused by solar wind pressure changes and the Kelvin-Helmholtz instability, *J. Geophys. Res.*, 108, 20-1, 2003.

Fedder, J. A., J. G. Lyon, S. P. Slinker, and C. M. Mobarry, Topological structure of the magnetotail as function of interplanetary magnetic field and with magnetic shear, *J. Geophys. Res.,* 100, 3613, 1995.

Goldstein, M.L, D.A. Roberts, A.V. Usmanov, Numerical simulation of solar wind turbulence, this issue.

Hasagewa, H. et al., Transport of solar wind into Earth's magnetosphere through rolled-up Kelvin-Helmholtz vortices, *Nature*, 430, 755, 2004.

Hughes, W.J., Magnetospheric ULF waves: a tutorial with a historical perspective, in *Solar Wind Sources of Magnetospheric Ultra-Low-Frequency Waves,* edited by M.J. Engebretson,
K. Takahashi, M. Scholer, AGU, Wash., D.C., 1994.

Kepko, L., H.E. Spence, and H.J. Singer, ULF waves in the solar wind as direct drivers of magnetospheric pulsations, *J. Geophys. Res.*, 29, 39-1, 2002.

Kessel, R.L., I.R. Mann, S.F. Fung, D. Milling, and N. Oconnell, Correlation of Pc5 wave power inside and outside the magnetosphere during high speed streams, *Ann. Geophys.*, 21, 1-13, 2003.

Kessel, R.L., et al, Comparison of high speed streams with and without large magnetic storms, manuscript in preparation, 2004.

Kokubun, S., T. Yamamote, M.H. Acuna, K. Hayashi, K. Shiokawa, and H. Kawano, The GEOTAIL magnetic field experiment, *J. Geomag. Geoelectr.*, 46, 7-21, 1994.

Lepping, R.P., M.H. Acuna, L.F. Burlaga, W.M. Farrell, et al., The Wind Magnetic Field Investigation, in The Global Geospace Mission, ed. C.T. Russell, **Kluwer** *Academic Publishers*, 207-229. 1995.

Li, X., D.N. Baker, D. Larson, M. Temerin, G. Reeves, S.G. Kanekal, The predictability of the magnetosphere and space weather, EOS, 361, 2003.

Mann, I.R., A.N. Wright, K.J. Mills, and V.M. Nakariakov, Excitation of magnetospheric waveguide modes by magnetosheath flows, *J. Geophys. Res.*, 104, 333-353, 1999.

Mathie, R.A., and I.R. Mann, A correlation between extended intervals of ULF wave power and storm-time geosynchronous relativistic electron flux enhancements,

Geophys. Res. Lett., **27**, 3261, 2000.

Miura, A, Anomalous Transport by Magnetohydrodynamic Kelvin-Helmholtz instabilities in the solar wind magnetosphere interaction, *J. Geophys. Res.*, 89, 801, 1984.

Miura, A, Kelvin-Helmholtz instability at the magnetospheric boundary: Dependence on the magnetosheath sonic Mach number, *J. Geophys. Res.*, 97, 10665, 1992.

Mukai, T. et al., Low Energy Particle Experiment (LEP), in p. 97, Geotail Prelaunch Report, ISAS, 1992.

Ogilvie, K.W., D.J. Chornay, R.J. Fritzenreiter, F. Hunsaker, et al., SWE, Comprehensive Plasma Instrument for Wind Spacecraft, in Global Geospace Mission, ed. C.T. Russell, **Kluwer Academic Pub.**, 55, 1995.

Otto, A., and D.H. Fairfield, Kelvin-Helmholtz instability at the magnetotail boundary: MHD simulation and comparison with Geotail observations, *J. Geophys. Res.*, 105, 21175, 2000.

Perreault, P and S.-I. Akasofu, Geophys. J. Roy. Astron. Soc., 54, 547, 1978.

Posch, J.L. et al., Characterizing the long-period ULF response to magnetic storms, *J. Geophys. Res.*, 108, 18-1, 2003.

Press, W.H., B.P. Flannery, S.A. Teukolsky, and W.T. Vetterling, Numerical Recipes, the art of scientific computing, Cambridge University Press, Cambridge, 1986.

Ramirez, Robert W., The FFT, Fundamentals and Concepts, Prentice-Hall, Inc., Englewood Cliffs, N.J., 1985.

Rostoker Gordon, et al., On the origin of relativistic electrons in the magnetosphere associated with geomagnetic storms, *Geophys. Res. Lett.*, 25, No. 19, 3701, 1998.

Sibeck, D.G., W. Baumjohann, R.C. Elphic, D.H. Fairfield, et al., The magnetospheric response to 8-minute period strong-amplitude upstream pressure variations, *J. Geophys. Res.*, 94, 2505, 1989.

Sibeck, D.G., T.-D. Phan, R.P. Lin, R.P. Lepping, T. Mukai, and S. Kokubun, A survey of MHD waves in the magnetosheath: International Solar Terrestial Program observations, *J. Geophys. Res.*, 105, 129, 2000.

Singer, H.J, L. Matheson, R.Grubb, A.Newman, and S.D.Bouwer, Monitoring Space Weather with GOES Magnetometers, SPIE Proceedings, Volume 2812, 1996.

Tsurutani, B.T. and W.D. Gonzalez, The causes of geomagnetic storms during solar maximum, EOS, 49, 1994.

Wright, A.N. and G.J. Rickard, A numerical study of resonant absorption in a magnetohydrodynamic cavity driven by a broadband spectrum, Astrophys. J., 444, 458-470, 1995.